Resistivity imaging in a fold and thrust belt using ZTEM and sparse MT data

David Alumbaugh[1*], Haoping Huang[1], Jennifer Livermore[1] and M. Soledad Velasco[1] present the results of a geophysical investigation of the northern Raton Basin in southern Colorado.

As part of a CO_2 reservoir exploration programme, NEOS acquired and analysed a variety of geophysical data within a ~2900 km^2 region of the northern Raton Basin of southern Colorado (Figure 1a). The purpose of the survey was to better define the basin architecture and identify structures that may serve as traps for the CO_2 gas. In addition to the Z-axis Tipper Electromagnetic (ZTEM) and magnetotelluric (MT) data discussed here, magnetic data were collected and publicly available ground gravity and satellite remote sensing data were analysed. We also had limited access to proprietary two-dimensional (2D) seismic and well data. Note that the acquisition area contains significant topography with elevations ranging from 1500 m above sea level in the basin to mountain peaks with elevations exceeding 4000 m.

Resolution analysis

A primary question in designing the electromagnetic (EM) data acquisition was how to maximize resolution in a cost effective manner. The area of interest is structurally complex, and the topography to the west makes ground access difficult. Land ownership in the area is a combination of private and government, with the State of Colorado, the US Forest Service, and the US Bureau of Land Management being the government agencies with jurisdiction over different tracks of land. In addition, Colorado has both surface and subsurface mineral rights owners, and thus two different permits must often be obtained to occupy a site. These factors made access to land difficult and the permitting process expensive. In fact, the MT permitting process took four months and was nearly as expensive as the data acquisition itself.

Because of the land access and permitting issues, as well as the large amount of terrain needing to be traversed during the geophysical survey, we decided to incorporate a dense airborne ZTEM survey along with the sparse MT stations. ZTEM measures the vertical magnetic field transfer function, or tipper, and thus is directly complimentary to the ground MT measurements. A ZTEM response will only be measureable in the presence of 2D or 3D structure which gives the measurement added spatial resolution in a structurally complex area. The strategy employed was to incorporate the airborne measurement to image structural variations in the upper 1000 m, and the sparse deeper sensing MT to map the deeper basin structure.

To demonstrate the advantage of collecting high-density airborne data along with sparse ground measurements in a fold and thrust belt regime, we have employed the model

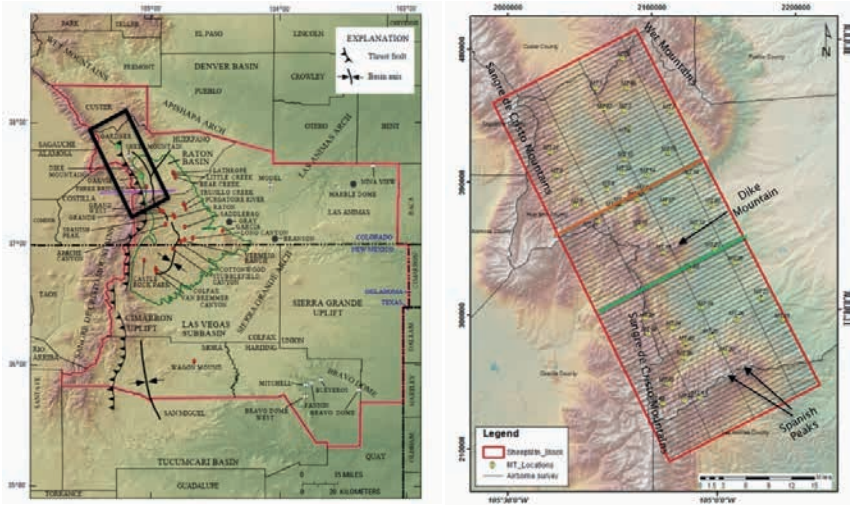

Figure 1 (a) Map of the northern New Mexico, southern Colorado area indicating the location of the exploration project as well as major thrust faults that are part of the Rocky Mountain fold and thrust belt (Higley, 2007). (b) Close-up of the survey region indicating the ZTEM flight lines along with MT stations. The orange and green lines represent the locations of two cross sections discussed below, and various mountains referenced in the text are highlighted.

[1] *NEOS.*

[*] *Corresponding author, E-mail: dalumbaugh@neosgeo.com*

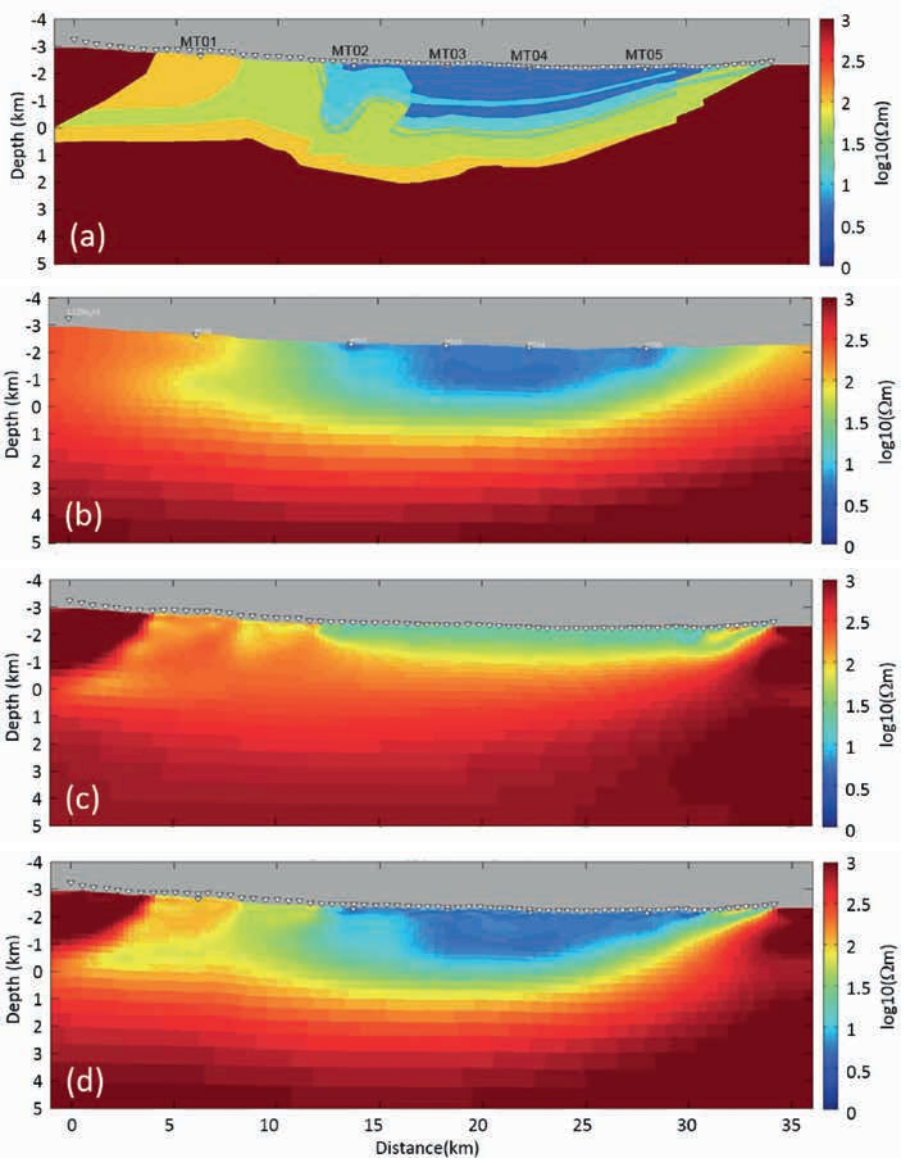

Figure 2 *(a) Resistivity model used in the resolution analysis of ZTEM and MT data. The simulation employed five ground MT stations shown in bold along with the seventy ZTEM airborne measurement locations designated by the small triangles. (b) Image resulting from inversion of five MT stations only. (c) Image resulting from inversion of ZTEM data only. (d) Image resulting from joint inversion of MT and ZTEM data.*

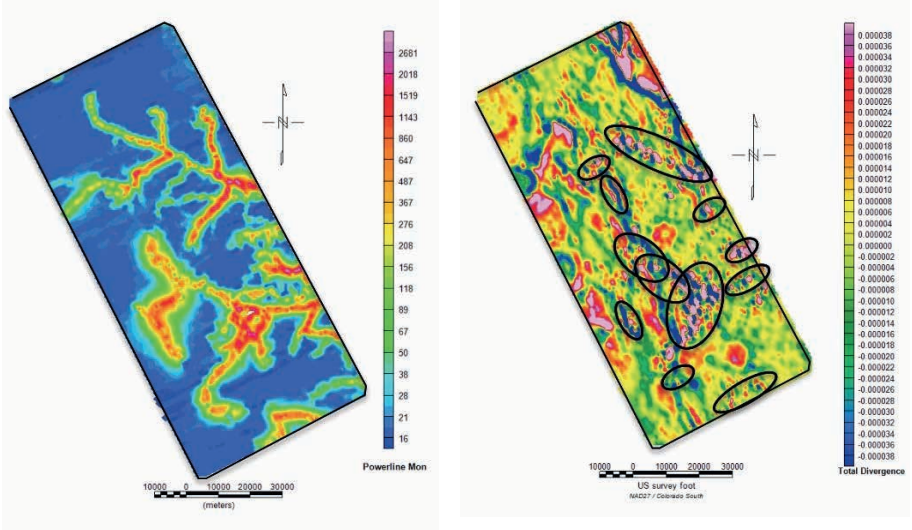

Figure 3 *(a) Powerline monitor with red responses representing large 60 Hz signal. (b) In-phase total divergence at 30 Hz with the black ellipses representing regions of high powerline response that also show oscillations in the measured ZTEM data. Much of the data within these regions were eliminated prior to inversion.*

shown in Figure 2a. This was derived partly from the cross sections of Roth (1983) as well as from the USGS Huerfano Park report by Johnson (1959). The resistivity of each unit was estimated depending on rock type using available well logs as well as geologic knowledge. Synthetic MT data were calculated for six frequencies per decade from 1 kHz down to 100 seconds at the five designated MT locations. The triangles above the earth surface represent locations where ZTEM results were calculated at 500 m station intervals using ZTEM frequencies of 30, 45, 90, 180, 360, and 720 Hz. Both the forward modelling and subsequent inversions employed the 2D finite element algorithm of Key (2012). We did not add synthetic noise to the data but did assume noise levels of 5% on the MT apparent resistivity and phase, and 0.01 on the ZTEM measurements which were deemed reasonable noise estimates based on the analysis of other data sets we were able to access. Because of the sparse nature of the ground measurements, a horizontal to vertical smoothing ratio of 10 was employed during the inversion to ensure lateral image continuity between the stations.

Figure 2b shows the resistivity image resulting from inversion of the five MT stations alone, while Figure 2c shows the results of inverting the ZTEM data only. Note that while the MT-only inversion maps the larger scale structure, the ZTEM-only inversion does a better job of imaging the lateral resistivity discontinuities. Likewise, the depth resolution of the ZTEM-only image in Figure 2c is poor with sensitivity limited to the upper 1 km. As shown in Figure 2d, when the two types of measurements are combined, the resulting image provides better resolution of the basin shape and depth, as well as the geometry of the basin bounding thrust faults. These simulations provided us with confidence that the combined ground and airborne surveys would yield superior results to ground acquisition alone given the aforementioned limitations to property access.

Data acquisition, quality, and preliminary analysis

Both the ZTEM and MT data were collected during mid-to-late summer of 2015 with data acquisition locations shown in Figure 1b. Helicopter ZTEM data acquisition by Geotech was hampered from a logistical standpoint by afternoon winds and thunderstorms which restricted flying times to the morning hours, and data quality wise by powerlines across the survey area which limited the usefulness of data in certain regions. Figure 3a displays a map of the 'Powerline Monitor' which Geotech provides as part of the data deliverables. Note that the units are relative and don't have meaning other than that larger red values are indicating close proximity to a powerline. Figure 3b displays a map of the real component of the 'total divergence' of the ZTEM data at 30 Hz calculated from the in-line and cross-line processed data as discussed in Lo and Zhang (2008). Closer inspection of the processed results within the regions enclosed by the black ovals indicate the data to be rapidly oscillating. Note that these locations also correlate to regions of high powerline response as shown in Figure 3a, thus identifying data that are so contaminated by 60 Hz cultural noise that they cannot be used for interpretation or inversion.

In Figure 4, we have replotted the in-phase component of the total divergence with fault, lineament, and dyke interpretations from the magnetic and gravity data overlain. In addition, we have muted the colour somewhat and added shaded-relief to emphasize structural trends in the data. In the overlay, black lines represent the location of interpreted northwest-southeast trending faults and northeast-southwest trending lineaments, and the purple lines represent the interpreted locations of intrusions and dykes. Note that even though the data still contain the rapid oscillations within the regions previously denoted to be affected by powerlines, there is a very strong correlation between the spatial trend of the ZTEM response and major mountain-front thrust fault features along the western half of the survey area, as well as the upper northeast corner. Also interesting is the sensitivity of the ZTEM data to volcanic centres in the region, such as the Dyke Mountain

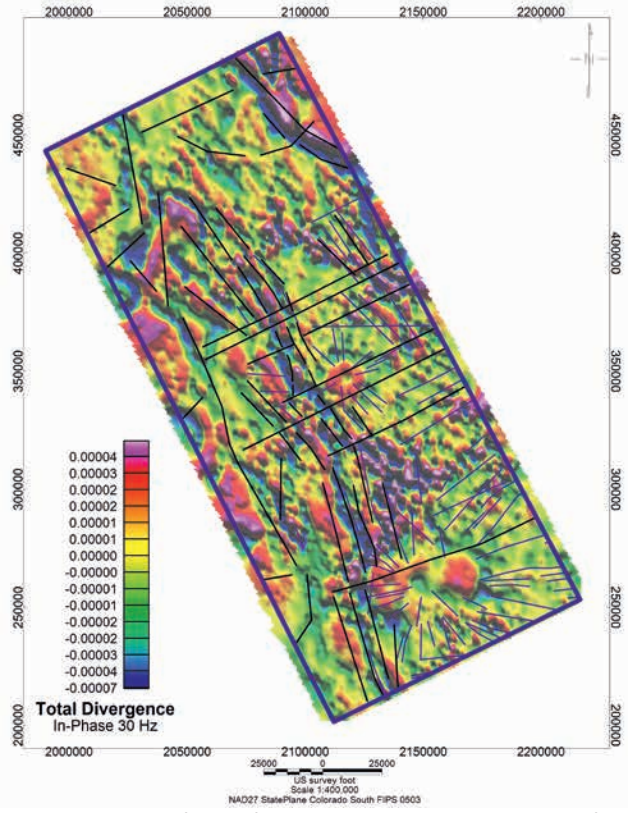

Figure 4 *Shaded-relief map of 30 Hz in-phase total divergence with fault (black lines) and dyke (purple lines) interpretations made from the magnetic and gravity data overlain. Note that the lateral dimensions are in feet rather than metres.*

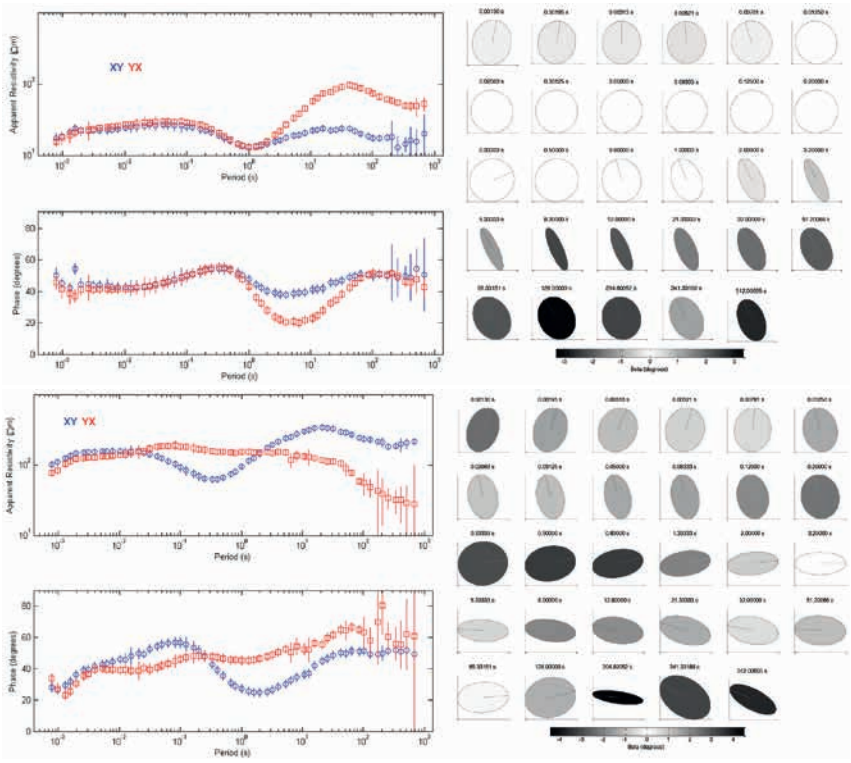

Figure 5 *Magnetotelluric data for (a) Station 29 in the southeast section of the survey area, and (b) Station 48 in the southwest section. The left side of each plot shows the apparent resistivity (top) and impedance phase (bottom) curves for each station, while the right side of each plot shows the phase tensor ellipses ranging from high frequency at the top to low frequency at the bottom.*

volcano just to the southeast of the centre of the survey area, and the Spanish Peaks volcanoes in the southern edge of the survey are imaged as circular features in Figure 4.

The MT acquisition was provided by Zonge International. Analysis of Figure 1b indicates significant gaps between the stations. In addition, one station had to be abandoned due to livestock and/or other animals repeatedly disturbing the site during acquisition. However, at the stations where data were able to be collected, the processed results tended to be of excellent quality down to a period of 100 seconds, with only two stations showing any signs of cultural noise contamination.

Because of the structural complexity of the area, the data ranged from being predominantly 1D to being very 3D in nature, and Figure 5 illustrates these extremes at two MT stations. Figure 5a is from Station 29 collected in the south-eastern corner of the survey area near the centre of the basin. The left-hand side of the figure are the apparent resistivity and impedance phase curves for the two off-diagonal modes of the impedance tensor, while the right-hand portion of Figure 5a shows the 'Phase Tensor Ellipses' (Caldwell et al., 2004) with highest frequencies at the top and lowest at the bottom. For a thorough description of what the various parameters of the phase tensor mean and how plots of the ellipse can be employed to evaluate the geologic complexity from an MT measurement the reader is referred to Jones (2012). The combination of the XY and YX modes overlapping each other in both apparent resistivity and phase down to 1 to 0.1 Hz along with the very circular nature of the phase tensor ellipse and low β values (grey shading of the ellipse) in this same frequency range indicate that the earth is predominantly 1D in the upper section. Note the β value is a direct indicator of three dimensionality, and thus a zero value indicates a 1D or 2D earth model. The general 1D structure that can be interpreted from the curves is that of a somewhat resistive (10 to 20 Ωm) near surface underlain by a more conductive zone which is further underlain by a resistor. At periods below 10 seconds the two modes of apparent resistivity and phase diverge, and the ellipticity and β values of the phase tensor increase. However, the β values in general stay at 2 or below, and the main diagonal of the ellipses are approximately aligned with the major geologic strike in the region. These two factors suggest that although at this station lower frequencies are sensing predominantly 2D geology rather than 1D, analysis with the 2D inversion code as described below should be adequate over most of the frequency range.

The curves displayed in Figure 5b are from a station located within the Sangre de Cristo Mountains on the western side of the survey region. Comparison of these data to those shown in Figure 5a indicate a significant level of structural complexity, even at the highest frequencies. Both modes of the apparent resistivity and phase curves diverge indicating at least 2D if not 3D structures present from the near surface to depth. The phase tensor ellipses exhibit non-circular behaviour even at the highest frequencies, and

the magnitude of the β parameter is most often greater than 2. Maybe most interesting is that the main axis of the phase tensor ellipse changes from high to low frequency indicating that different frequency data are sensing different geologic strike directions. All of these together indicate that the geological structure surrounding this station is very complicated, and that the data need to be handled properly during the inversion stage in order to yield meaningful results.

Data editing, inversion methodology, and results

Ultimately, the goal of processing the data collected during the EM survey was to produce a 3D resistivity volume from which structural intepretations could be made. Currently, we are using the aforementioned 2D inversion code of Key (2012), and full 3D inversion is proposed for future work. Because the data clearly exhibit 3D attributes, the use of the 2D code required additional processing and editing prior to inversion. In this regard, the ZTEM data did not need any rotation applied as the flight line direction was chosen to be perpendicular to the regional geological strike. However, to satisfy the 2D approximation only the data corresponding to a tipper aligned with the flight-line directions were used. The other processing step applied to the ZTEM data was to manually eliminate those measurements that showed signs of powerline contamination such as those highlighted within Figure 3b. One last note to mention is that the ZTEM data were decimated from approximately a 6 m station spacing as delivered by Geotech to a 500 m station spacing in order that the inversion grid did not have to be discretized to a level that would overload the available computer memory.

The first pre-inversion processing step for the MT data was to rotate the data to the same direction as the ZTEM flight lines. Next, data showing large 3D effects were deleted for the inversion process. This was accomplished through analysis of the Swift Skew, the phase tensors described in Figure 5, and the impedance polar diagrams for each station and frequency (see Jones (2012) for a description of how these parameters can be used to identify structural dimensionality). If any of these parameters suggested the presence of a significant 3D structure, those particular data were not used in the 2D inversion. In addition, the main diagonal of the impedance tensor could not be used as these parameters are only non-zero in the presence of 3D geology. This resulted in less than half of the processed MT data being used in the 2D inversion.

In total, 82 lines of ZTEM data were collected, all of which were inverted. To incorporate the MT data, stations within 2 km distance of a given flight line were included. Although this implies the majority of lines have at least one ground station associated with them, analysis of Figure 1b indicates there will be many lines that have no MT data for inversion. As demonstrated in Figure 2c, these lines will suffer from limited depth senistivity and resistivity resolution which can result in the images for two adjacent lines looking very different, which is not geologically reasonable. To circumvent this problem, we developed a 'line-to-line' model constrained inversion approach. Similar in nature to the 'laterally contrained' inversion technique of Auken and Christiansen (2004), this method includes a 'closest model' formulation in the cost function to ensure that each line is as close to adjacent lines in terms of resistivity structure as

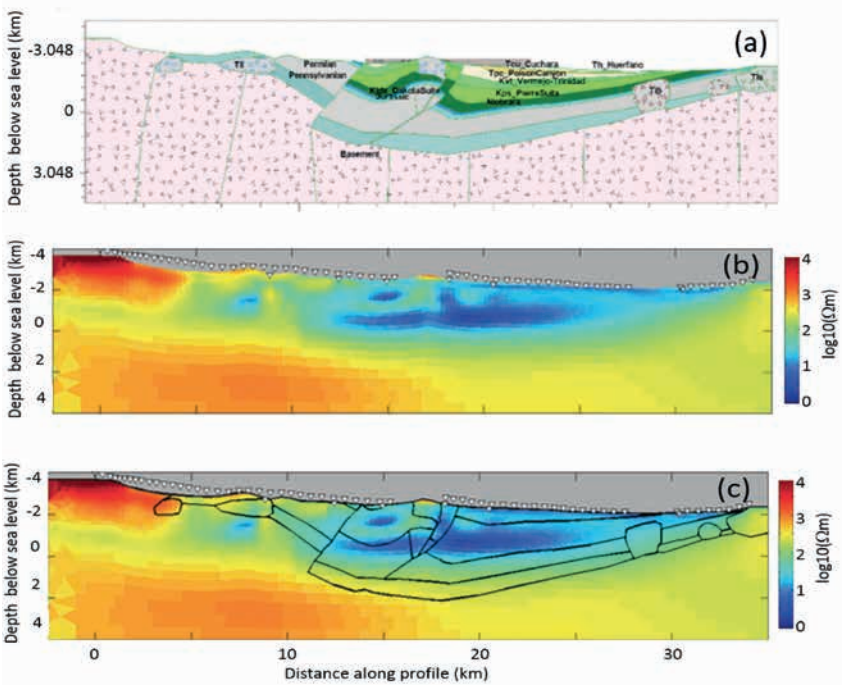

Figure 6 *(a) Geologic profile and (b) resistivity image along the orange line shown in Figure 1b. (c) The resistivity image in (b) with the addition of structural boundaries shown in the geologic cross section of (a) overlain.*

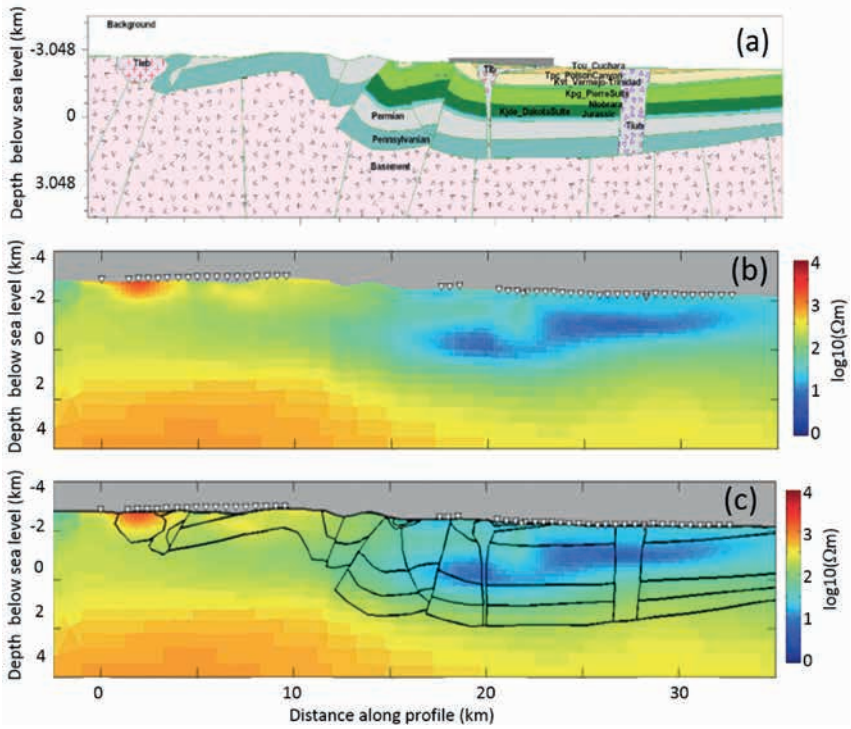

Figure 7 *(a) Geologic profile and (b) resistivity image along the green line shown in Figure 1b. (c) The resistivity image in (b) with the addition of structural boundaries shown in the geologic cross section of (a) overlain.*

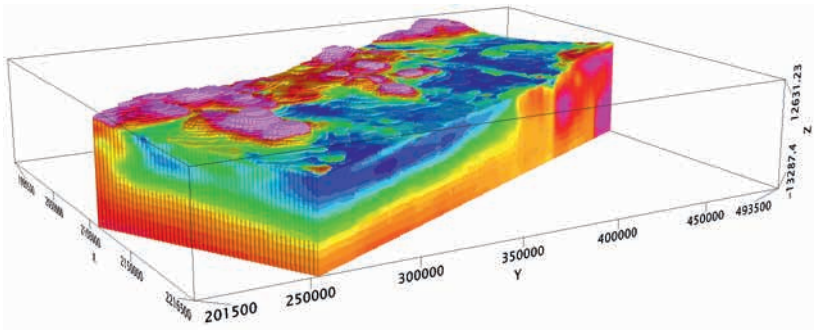

Figure 8 *3D resistivity volume constructed via Kriging of the 82 2.5D inversions along each of the ZTEM flight lines shown in Figure 1b. Note that the dimensions in this plot are in feet rather than metres.*

the data will allow, thus providing coherency in the images perpendicular to the direction of the flight lines.

The results of applying this inversion approach are shown for profiles along the orange and green lines in Figure 1b and in Figures 6 and 7, respectively. Figure 6 is for a profile that has six MT stations associated with it, and a minimal amount of ZTEM data removed due to powerline contamination. Thus, this profile is one of the better data-constrained sections. The top plot is a geologic cross section developed through the analysis of the seismic, gravity, magnetic and well log data, the second image the resistivity inversion results, and the third image the resistivity inversion with major stratigraphic boundaries, faults, and intrusions from the cross section in 6a overlain. Note that the inversion provides definition of conductive sediments filling the basin and terminating against the western thrust fault. Analysis of well logs suggest that the most conductive zones in the image are due to a thick sequence of low resistivity shales within the Cretaceous Pierre group.

The results in Figure 7 are along the green line in Figure 1b which only has two MT stations associated with it, and has a large gap in the ZTEM data due to powerline contamination. This leads to poorer resolution in identifying the fault location when compared to the result in Figure 6. At the same time, the resistivity image still provides a good depiction of the basin geometry.

As mentioned above, the ultimate goal of the EM data collection and inversion was to produce a 3D resistivity volume which can aid in interpretation. This was accomplished by interpolating between the 82 2D inversion lines using a Kriging algorithm. The resulting 3D volume is shown in Figure 8 as viewed from the southeast. Note the definition of the conductive sediments filling the Raton Basin as well as the more resistive Sangre de Cristo Mountains to the

west and resistive peaks in the basin corresponding to various volcanic outcrops.

Given the general lack of good quality 2D seismic data as well as 3D coverage, one of the important interpretation aspects of the Raton Basin project was to better define the shape of the basin and constrain the depth to basement. In the end, the combined ZTEM/MT survey proved invaluable in achieving the latter goal; the potential field data proved

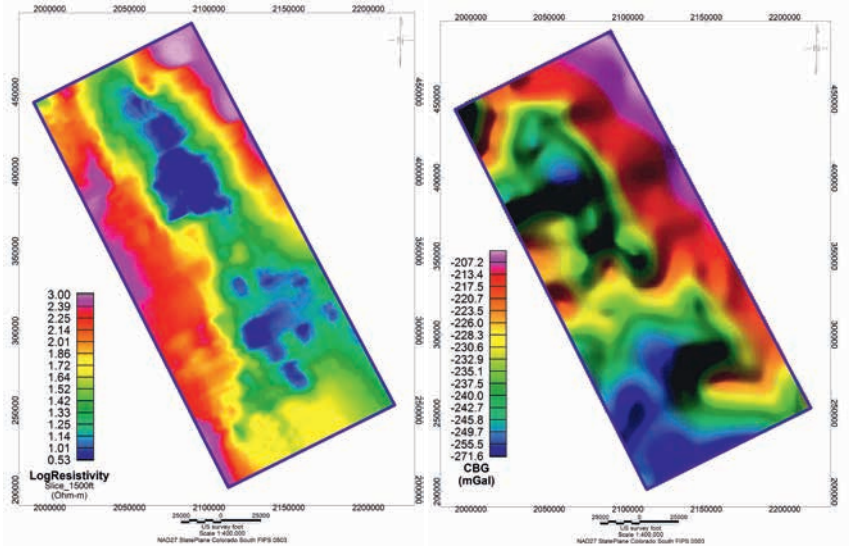

Figure 9 *(a) Resistivity depth slice at approximately 500 m above sea level from the voxel volume shown in Figure 8. (b) Complete Bouguer Gravity anomaly. Note that the dimensions in these plots are in feet rather than metres.*

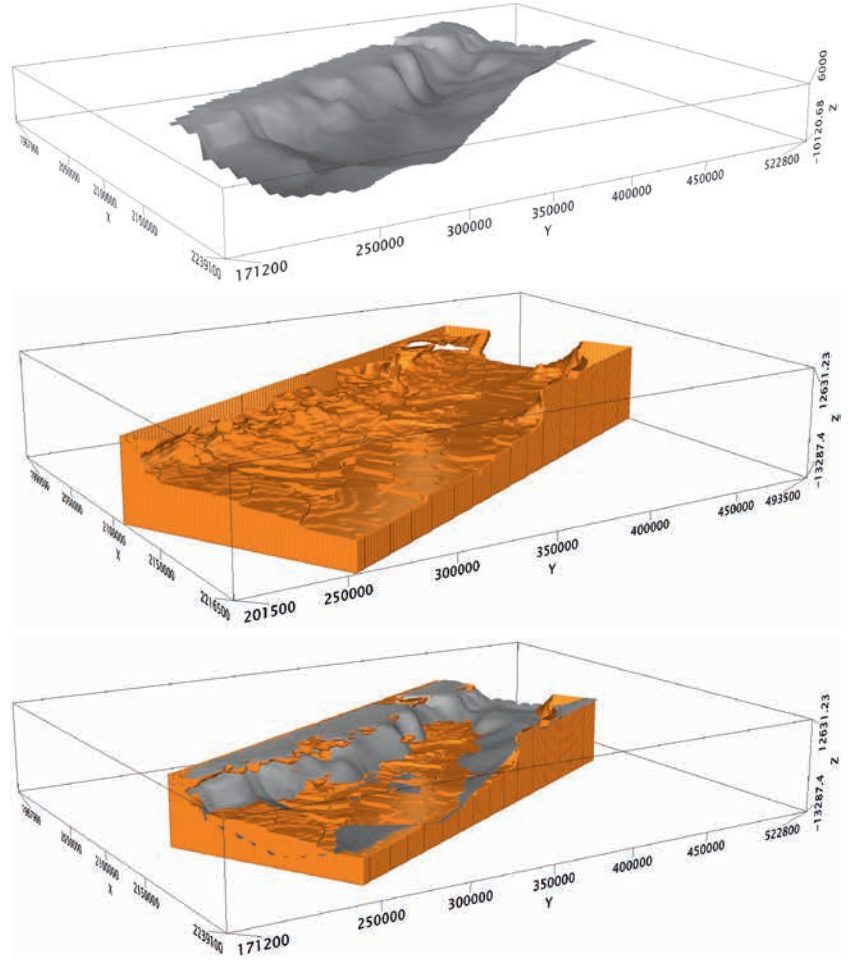

Figure 10 *(a) View from the southeast of the basement-sediment interface as interpreted from all geophysical data excluding the ZTEM and MT data, as well as published geological studies. (b) The 200 Ωm isosurface extracted from the resistivity volume shown in Figure 8. (c) Figure combining the surfaces shown in (a) and (b). Note that the dimensions in these plots are in feet rather than metres.*

difficult to provide easy-to-interpret depth-to-basement estimates due to the numerous intrusions, making analysis nearly impossible.

In Figure 9, we analyse the resistivity image in terms of providing insight into the general shape of the basin. Figure 9a represents a resistivity depth slice at approximately 500 m above sea level. Here, low resistivity values (blue) represent sedimentary rocks filling the basin while high resistivity values (red) represent basement rocks. For comparison in Figure 9b, we plot the Complete Bouguer Gravity anomally generated from public domain gravity data that were downloaded from the University of Texas at El Paso. In general, the two look similar in terms of identifying the basin location and shape. Two sub-basins are observed in both datasets, represented by lower resistivity and lower density (blue colours in both figures). Rock samples and data analyses have shown that the rocks outcropping in the Sangre de Cristo Mountains to the west are lower density than those outcropping in the Wet Mountains to the east. Also, many intrusions and extrusive volcanic features in the central and southeastern part of the study area are likely to be causing the density highs observed in these regions. Therefore, direct intepretation of Figure 9b in terms of basin shape without significant modelling effort is likely to produce an interpretation that is skewed towards the basin being farther west than it really is.

Figure 10 compares depth to basement as interpreted using all available data other than the EM data (Figure 10a) to the 200 Ωm isosurface extracted from the resistivity voxel in Figure 8 (Figure 10b). Note all images here have been clipped at 1800 m above sea level so that the near surface-high resistivity zones do not obstruct the view of the basement surface at depth. In Figure 10c the interpreted surface is included along with the resistivity isosurface. Note that to the south the interpreted basement is deeper than the isosurface, while to the north, it is shallower. Inspection of Figure 1b shows that these two regions are lacking in MT stations due to the aforementioned permitting and access issues, and thus, there is limited depth sensitivity to the basement in these locations. However, analysis also shows that over the rest of the basin the 200 Ωm isosurface does well in mimicking the interpreted basement interface.

Conclusions

A combined dense airborne ZTEM and sparse ground MT data set collected in the northern Raton Basin of southern Colorado has been inverted for 82 profiles using a 'line-to-line' constrained 2D inversion scheme. The 82 2D resistivity profiles have been interpolated using Kriging techniques to produce a 3D resistivity volume. The resulting images and voxel provide valuable information about basin geometry, including the lateral termination of Jurassic and younger clastics against thrust faults bounding the western side of the basin. In addition, the choice of an appropriate resistivity cut-off value of 200 Ωm agrees well with the interpreted basement depth across most of the survey region. Because a 2D inversion scheme was employed, much of the data were not included in the inversion process owing to 3D effects. Thus, a full 3D inversion that includes all of the data will be perform in the future, and the results evaluated and compared against this approximate technique.

Acknowledgements

The authors would like to thank NEOS for permission to publish this work, and Geotech LTD and Zonge International for collecting the EM data. The authors would also like to thank Joshua Poirier, Maggie Baber, Nathan Skitt, Stefano Mazzoni, Craig Beasley, and Don Chitwood for their valuable contributions to this study. Lastly, we would like to thank David Myer of BlueGreen Geophysics, and Kerry Key of the Scripps Institute of Oceanography for their support in using the MARE2DEM inversion code as well as the routines that plot the output and manipulate the data.

References

Auken, E., and Christiansen, A.V. (2004). Layered and laterally constrained 2D inversion of resistivity data. *Geophysics*, **69**(3) 752-761.

Caldwell, G., Bibby, H., Grant, H, and Brown, C. (2004). The magnetotelluric phase tensor. *Geophysical Journal International*, **158**(2), 457-469.

Higley, D.K. (2007). Petroleum systems and assessment of undiscovered oil and gas in the Raton Basin–Sierra Grande Uplift Province, Colorado and New Mexico. *In:* Higley, D.K., *Petroleum Systems and Assessment of Undiscovered Oil and Gas in the Raton Basin–Sierra Grande Uplift Province, Colorado and New Mexico — USGS Province 41*. U.S. Geological Survey Digital Data Series DDS–69–N, ch. 2.

Johnson, R.B. (1959). Geology of the Huerfano Park Area, Huerfano and Custer Counties Colorado. *USGS Geological Survey Bulletin* 1071-D.

Jones, A. (2012). Distortion of magnetotelluric data: its identification and removal: *In* Chave, A., and Jones, A., Editors, *The Magnetotelluric Method – Theory and Practice*. Cambridge University Press. 219-302.

Key, K. (2012). Marine EM inversion using unstructured grids: a 2D parallel adaptive finite element algorithm; Expanded abstracts of the *SEG Annual Meeting*, SEG-2012-1294.

Lo, B. and Zhang, M. (2008). Numerical modeling of Z-TEM (airborne AFMAG) responses to guide exploration strategies. *SEG Annual Meeting*, SEG-2008-1098.

Roth, G. (1983). Sheep Mountain and Dike Mountain Fields, Huerfano County, Colorado; a source of CO_2 for enhanced oil recovery. *In: Four Corners Geological Society – Oil and Gas Fields of the Four Corners Area Volume* III, 740-744.